The Astrophysical Journal, 877:90 (8pp), 2019 June 1 https://doi.org/10.3847/1538-4357/ab1078

Discovery of a New Class I Methanol Maser Transition at 266.8 GHz

Xi Chen[1,2], Simon P. Ellingsen[3], Zhi-Yuan Ren[4], Andrej M. Sobolev[5], Sergey Parfenov[5], and Zhi-Qiang Shen[2,6]
[1] Center for Astrophysics, GuangZhou University, Guangzhou 510006, People's Republic of China; chenxi@gzhu.edu.cn
[2] Shanghai Astronomical Observatory, Chinese Academy of Sciences, Shanghai 200030, People's Republic of China; chenxi@shao.ac.cn
[3] School of Natural Sciences, University of Tasmania, Hobart, TAS 7001, Australia
[4] National Astronomical Observatories, Chinese Academy of Science, Datun Road. A20, Beijing, People's Republic of China
[5] Ural Federal University, 19 Mira Street, 620002 Ekaterinburg, Russia
[6] Key Laboratory of Radio Astronomy, Chinese Academy of Sciences, Nanjing, JiangSu 210008, People's Republic of China
Received 2018 December 27; revised 2019 February 20; accepted 2019 March 14; published 2019 May 29

Abstract

We report the detection of a new class I methanol maser candidate from the 5_2-4_1 *E* transition (266.8 GHz). This methanol transition has been detected toward a nearby high-mass star-forming region G352.630-1.067 (distance ~0.7 kpc), in Submillimeter Array (SMA) observations. The new candidate transition has a similar spatial distribution as the 4_2-3_1 *E* (218.4 GHz) and $8_{-1}-7_0$ *E* (229.7 GHz) transitions, which are known class I maser transitions. Thermal methanol emission in this source is confined to a central hot core, while the three class I maser transitions are detected in two additional regions. These two maser-only emission regions are clearly associated with shocked gas traced by 2 μm *Ks*-band and thermal $v = 0$, $J = 5-4$ SiO molecular emission. In contrast to the thermal methanol emission from the hot core, the three class I maser transitions show an positive trend in the rotation diagram for the two maser regions. Large velocity gradient modeling of the 266.8, 218.4, and 229.7 GHz transitions shows that the 266.8 GHz transition can be a maser for a wide range of conditions. The intensity ratios for the three methanol transitions detected in maser regions can be reproduced under conditions that are typical for class I methanol maser sites. These facts all support the hypothesis that the detected emission from the 266.8 GHz methanol (5_2-4_1 *E*) transition is masing.

Key words: ISM: jets and outflows – ISM: molecules – masers – stars: formation

1. Introduction

Methanol maser emission is a very common phenomenon in our Galaxy (e.g., Green et al. 2009; Chen et al. 2014; Yang et al. 2017). Methanol masers are empirically divided into two classes, known as class I and class II (Menten 1991). The two classes of methanol masers are most commonly found associated with high-mass star-forming regions (HMSFRs) (Sobolev et al. 2005), although some class I methanol masers are known to be associated with low-mass star formation regions (e.g., Kalenskii et al. 2006, 2010; Gan et al. 2013) and sites of cloud–cloud collisions with and without star formation (e.g., Salii et al. 2002; Sjouwerman et al. 2010). Class I methanol masers have a collisional source of pumping (Sobolev & Strelnitskii 1983; Cragg et al. 1992), and they are commonly produced by mild shocks driven into molecular clouds by protostellar outflows from high- or low-mass stars, expanding H II regions (e.g., Voronkov et al. 2010a; Chen et al. 2011), expanding supernova remnants (Pihlström et al. 2014), expanding envelopes of the late type stars (Nakashima et al. 2015), and rapidly moving cloudlets (Voronkov et al. 2010b). According to the pumping theory, class II methanol masers get their energy from the infrared radiation in vicinities of young high-mass stars, while class I masers appear when the radiation density is much lower, hence, at larger distances from the stars (e.g., Sobolev et al. 2007). Observations also show that typically the Class II masers are found close to (within 1″) the exciting high-mass protostars (Ellingsen 2006; Caswell et al. 2010), whereas the class I masers are usually offset by a much larger distance from the protostar (0.1–1 pc; e.g., Kurtz et al. 2004; Cyganowski et al. 2009; Voronkov et al. 2014; McCarthy et al. 2018).

Between the 2 classes, there are more than 30 different methanol transitions that have been observed to show maser emission in interstellar environments, covering a wide wavelength range from centimeter to millimeter wavelengths (Cragg et al. 2005). The methanol maser transitions that have been well studied to date are those at lower frequencies (<100 GHz), such as the 6.7 and 12.2 GHz class II transitions (e.g., Breen et al. 2010; Green et al. 2017), and the 9.9, 36, 44, and 95 GHz class I transitions (e.g., Voronkov et al. 2010a, 2014; Chen et al. 2011, 2013a; Yang et al. 2017). Identifying and searching for new methanol maser transitions provides important information that can be used to constrain the physical conditions of the regions in which the masers are located. A number of searches to test maser model predictions have been undertaken in recent years (Chipman et al. 2016); however, most of them have been focused on low-frequency transitions such as the 23.4 GHz class I transition (e.g., Voronkov et al. 2011) and the 37.7, 38.3, and 38.5 GHz class II transitions (Ellingsen et al. 2018). However, the identification of new methanol maser transitions at higher frequencies is more important to provide constraints on the physical conditions over a wider frequency range. Interferometric instruments at millimeter and submillimeter wavelengths, such as the Atacama Large Millimeter/submillimeter Array (ALMA) and the Submillimeter Array (SMA), are able to efficiently detect new methanol maser transitions at higher frequencies. This is because the combination of wide bandwidth, sensitivity, and angular resolution enables efficient observations of a larger number of molecular lines than was

Table 1
Details of the Detected Methanol Transitions

Methanol Component (1)	Frequency (GHz) (2)	Transition (3)	E_u/k (K) (4)	$S\mu^2$ (D^2) (5)	V_{LSR} (km s^{-1}) (6)	ΔV (km s^{-1}) (7)	$\int T_B dV$ (K km s^{-1}) (8)	T_B (K) (9)	Size (arcsec, arcsec, deg) (10)
M1	218.4401	4_2-3_1E	37.5	3.477	−2.5(0.1)	3.9(0.2)	7.5(0.4)	1.79(0.15)	4.2 × 1.3 @ −12
	229.7588	$8_{-1}-7_0E$	81.2	5.048	−2.3(0.1)	5.6(0.3)	9.3(0.4)	1.56(0.10)	3.9 × 1.0 @ −10
	266.8381	5_2-4_1E	49.1	3.848	−2.5(0.1)	5.5(0.3)	13.4(0.7)	2.28(0.16)	2.1 × 0.8 @ −17
M2	218.4401	4_2-3_1E	37.5	3.477	1.9(0.1)	1.3(0.1)	2.4(0.2)	1.75(0.23)	7.5 × 4.2 @ −30
	229.7588	$8_{-1}-7_0E$	81.2	5.048	1.1(0.1)	1.5(0.0)	9.9(0.2)	6.05(0.22)	8.2 × 4.6 @ −19
	266.8381	5_2-4_1E	49.1	3.848	0.9(0.1)	2.1(0.1)	3.6(0.2)	1.62(0.15)	4.0 × 1.7 @ −7
M3	218.4401	4_2-3_1E	37.5	3.477	−3.6(0.4)	8.0(1.0)	2.4(0.4)	0.24(0.09)	4.9 × 4.1 @ −84
	229.7588	$8_{-1}-7_0E$	81.2	5.048	−4.6(0.6)	12.2(1.9)	6.0(1.1)	0.46(0.11)	3.7 × 1.3 @ −10
	266.8381[a]	5_2-4_1E	49.1	3.848	−2.5(0.6)	11.9(2.2)	6.1(1.1)	0.48(0.12)	3.5 × 1.4 @ −10
	...	...	...	...	−2.1(0.1)	1.7(0.4)	1.6(0.2)	0.86(0.22)	...

Notes. Column (1): label for the methanol emission regions detected in the current SMA observations. Columns (2)–(5): the corresponding frequency, upper level energy, the quantum numbers of the transitions, and product of the total torsion-rotational line strength and the square of the electric dipole moment for each methanol transition, respectively. Columns (6)–(9): the line center velocity V_{LSR}, the FWHM line width ΔV, the integrated intensity $\int T_B dV$, and the peak brightness temperature T_B, determined from Gaussian fits to the line profile extracted from the peak position of the methanol emission. Column (10): the size and position angle of the component from a beam de-convolution, assuming Gaussian distributions.
[a] For this transition, we used two Gaussian features to fit the line profile toward M3.

previously possible with single-dish facilities such as the SEST (e.g., Ellingsen et al. 2012). This is demonstrated by the recent discovery with ALMA of new methanol maser lines from the $9_{-1}-8_0$ E (278.3 GHz class I; Yanagida et al. 2014) and the 14_1-14_0 A^{-+} (349.1 GHz class II; Zinchenko et al. 2017) transitions. Considerations of the maser pumping predict new detections in the high-frequency domain (see, e.g., Cragg et al. 2005; Voronkov et al. 2012; Leurini et al. 2016).

In this paper, we report SMA observations that have resulted in the detection of a new class I methanol maser from the 5_2-4_1 E transition at a frequency of 266.8 GHz. This new maser transition was detected in observations toward the HMSFR G352.630-1.067, which has recently been shown to be the second closest such region at a distance of about 0.7 kpc (Chen et al. 2019).

2. Observations

The observations toward the HMSFR G352.630-1.067 were made with the SMA[7] on 2017 August 3, with the array in its compact configuration. The phase tracking center was placed at the position of the 6.7 GHz methanol maser (α = 17:31:13.91, $\beta = -35$:44:08.7; J2000), which was obtained from the Methanol Multibeam (MMB) project (Caswell et al. 2010). The calibration of the time-dependent antenna gains was performed by regular observations of the quasar 1700-261. The quasar 3C454.3 was observed to calibrate the bandpass response and the absolute flux density was obtained from observations of Neptune and Titan.

The SWARM correlator was used in dual receiver mode with an 8 GHz bandwidth per sideband. With the 230 GHz receiver the setup covered the frequency ranges 213.5–221.5 GHz and 229.5–237.5 GHz, while the 240 GHz receiver was used to observe the frequency ranges 265.0–273.0 GHz and 281.0–289.0 GHz. The spectral channel width was about 0.5 MHz, corresponding to a velocity resolution of ∼0.7 km s^{-1} at 230 GHz, and ∼0.5 km s^{-1} at 285 GHz. In total, 20 methanol lines were detected by these SMA observations. Two known class I maser transitions, the 4_2-3_1 E (218.4 GHz; Hunter et al. 2014) and $8_{-1}-7_0$ E (229.7 GHz; Slysh et al. 2002), and one class I maser candidate transition, 5_2-4_1 E (266.8 GHz; reported here), were covered in these observations. In this paper, we focus primarily on the three maser lines and the data for the other thermal emission from methanol and other species will reported in a future paper. The details of the rest frequencies and electronic properties of the three class I methanol transitions are summarized in Table 1.

The visibility data were calibrated using the IDL superset MIR.[8] The imaging and analysis were carried out in MIRIAD.[9] The synthesized beam size, i.e., the angular resolution of the image data, was approximately 5.″8 × 2.″4 at 230 GHz and 4.″7 × 1.″9 at 285 GHz, with a position angle of −12.°3 northwest. The rms noise in a spectral channel was 50 mJy $beam^{-1}$ for the molecular line data.

3. Results

3.1. Integrated Intensity Images and Spectra of Methanol

Figure 1 shows the integrated intensity images for the three class I methanol transitions detected toward G352.630-1.067 in the current SMA observations, the 4_2-3_1 E (218.4 GHz), $8_{-1}-7_0$ E (229.7 GHz) and 5_2-4_1 E (266.8 GHz) lines. All the three methanol transitions are detected toward this source for the first time. It can clearly be seen that all three transitions are detected toward the phase tracking center and thus are associated with the region where the class II 6.7 GHz methanol maser arises. Hereafter, we refer to this central molecular emission region as "M1." The methanol emission from M1 has a compact structure, suggesting that it originates from a small region and is not resolved by the current SMA observations. Therefore, an upper limit on the angular size of M1 is ∼3″

[7] The Submillimeter Array is a joint project between the Smithsonian Astrophysical Observatory and the Academia Sinica Institute of Astronomy and Astrophysics, and is funded by the Smithsonian Institution and the Academia Sinica.

[8] See https://www.cfa.harvard.edu/~cqi/mircook.html.

[9] http://www.cfa.harvard.edu/sma/miriad, http://www.astro.umd.edu/~teuben/miriad

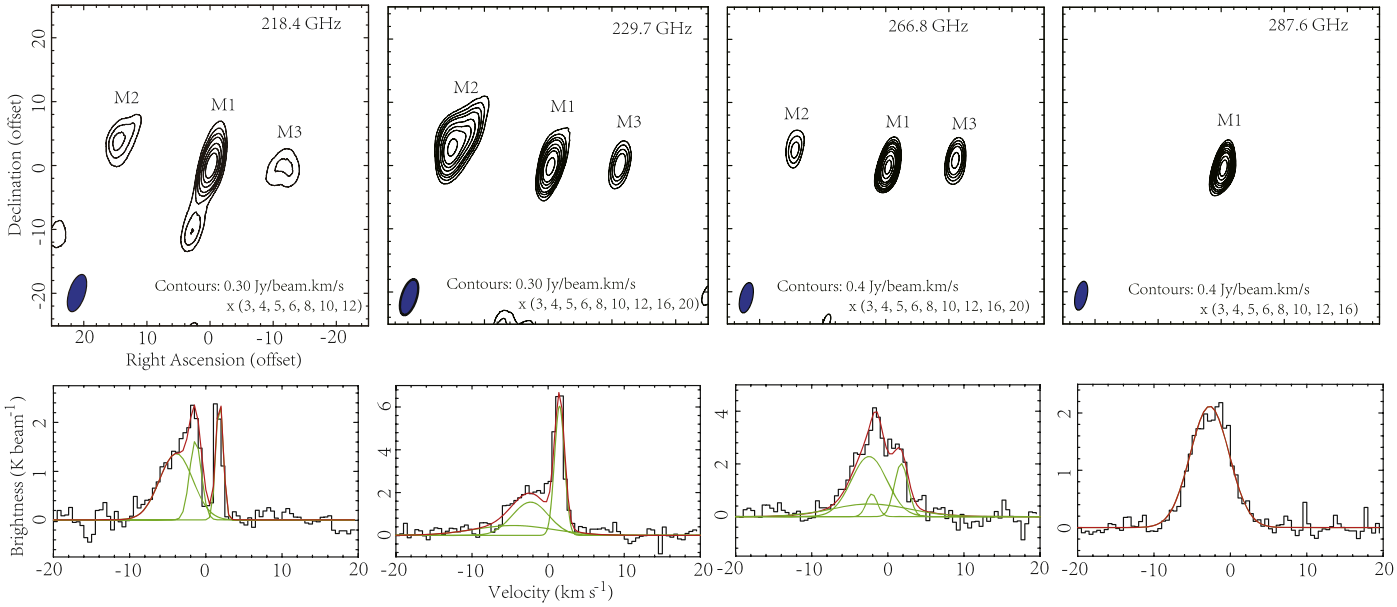

Figure 1. Images of the integrated emission and spectra of the methanol transitions detected in the SMA observations. The left three panels are given for the three class I methanol maser transitions at 218.4, 229.7, and 266.8 GHz. For comparison, an example of the thermal methanol emission at the 287.6 GHz transition is shown in the right panel. For each transition, the integrated methanol emission is in black contours with contour level values shown in the bottom of each panel. The synthesized beam for each image is shown in the bottom left corner. The methanol spectrum extracted toward the peak position of the integrated emission is shown in the corresponding lower panel. For the three class I maser transitions, the methanol spectra are given by summing the emission toward the peak positions of the three components M1, M2, and M3. A Gaussian fit to a single component is shown with a green profile for these transitions.

(corresponding to a linear size of ∼2000 au for a distance of 0.7 kpc). In addition to the methanol emission associated with the M1 region, we detect emission from two other sites in the three transitions. One of these is to the east (labeled as M2), and the other to the west of M1 (labeled as M3). These two regions are offset by 10–17 arcsec (7000–12,000 au or ∼0.05 pc) from M1. Figure 1 shows that the emission from M2 is extended compared to the synthesized beam size of the 218.4 and 229.7 GHz transitions, but it is compact for the 266.8 GHz transition. In contrast, M3 is relatively compact for all three methanol transitions where emission is detected. The fitting results for the beam-deconvolved sizes of the three components assuming Gaussian distributions (listed in Table 1) support this.

The spectra for each of the detected methanol transitions is shown in the bottom panels of Figure 1. The spectra are constructed from a combination of summing the three spectral features toward the peak positions of the three components. A single Gaussian can be fitted to the methanol spectrum for each component in each transition, with the exception of the 5_2-4_1 E (266.8 GHz) transition toward M3, where two Gaussian components were required (see below). The fitted parameters are given in Table 1. For M1, the three maser transitions show a similar line profile with peak velocities at ~-3 km s^{-1} and line widths of $\sim$5 km s^{-1}. The peak brightness of the transitions detected toward M1 ranges between 1.6 K beam^{-1} (229.7 GHz) and 2.3 K beam^{-1} (266.8 GHz).

For the M2 emission, all three methanol transitions show similar profiles, with a narrow line width ($\sim$1.5 km s^{-1}) at peak velocity of $\sim$1 km s^{-1}. The strongest emission toward M2 is detected from the 229.7 GHz transition, which has a peak brightness of 6.0 K beam^{-1}. The other two transitions (218.4 and 266.8 GHz) have a similar peak brightness of 1.7 K beam^{-1}. For M3, all three detected methanol transitions show a broad profile ($\sim$10 km s^{-1}). In addition, the 266.8 GHz emission also shows a narrow spectral feature (line width of 1.7 km s^{-1} at peak velocity of -2 km s^{-1}) overlaid on the broad spectral emission. Because of this we have used two Gaussian profiles to fit this transition toward M3. To enable a direct comparison of the methanol spectra from the three class I methanol transitions toward M2 and M3, we have plotted their spectra toward each of the components in the right panel of Figure 2. From Figure 1, we can also see that there is another methanol component in the 4_2-3_1 E (218.4 GHz) transition toward the southeast of M1, with an offset of 10″. This component does not show emission from any of the other methanol transitions.

For comparison, in the right panel of Figure 1 we present an image of the integrated emission and spectrum of the thermal methanol emission from the 6_1-5_1 A^+ (287.6 GHz) transition detected in the current SMA observations. As for the 287.6 GHz transition, all the other thermal methanol transitions were only detected toward M1. No emission from any of the thermal methanol transitions is detected toward M2 and M3, suggesting that their physical conditions are very different from M1 and supporting the hypothesis that the methanol emission toward M2 and M3 is due to masing (see discussion in Section 4.1).

3.2. Comparison with Shock Gas Tracers

Class I methanol masers are associated with mild shocks and to further investigate the possible presence of shocks in the G352.630-1.067 region we created an image of the integrated emission from the thermal SiO $v = 0$ $J = 5-4$ (217.105 GHz) transition. This transition was covered in the current SMA observations, and the left panel of Figure 2 shows it overlaid on the 2MASS K_s band and the integrated 5_2-4_1 E (266.8 GHz) methanol emission. The uncertainty in relative positions between the 266.8 GHz methanol, the 2 μm and the SiO maps is less than 1″, considering the position errors of their

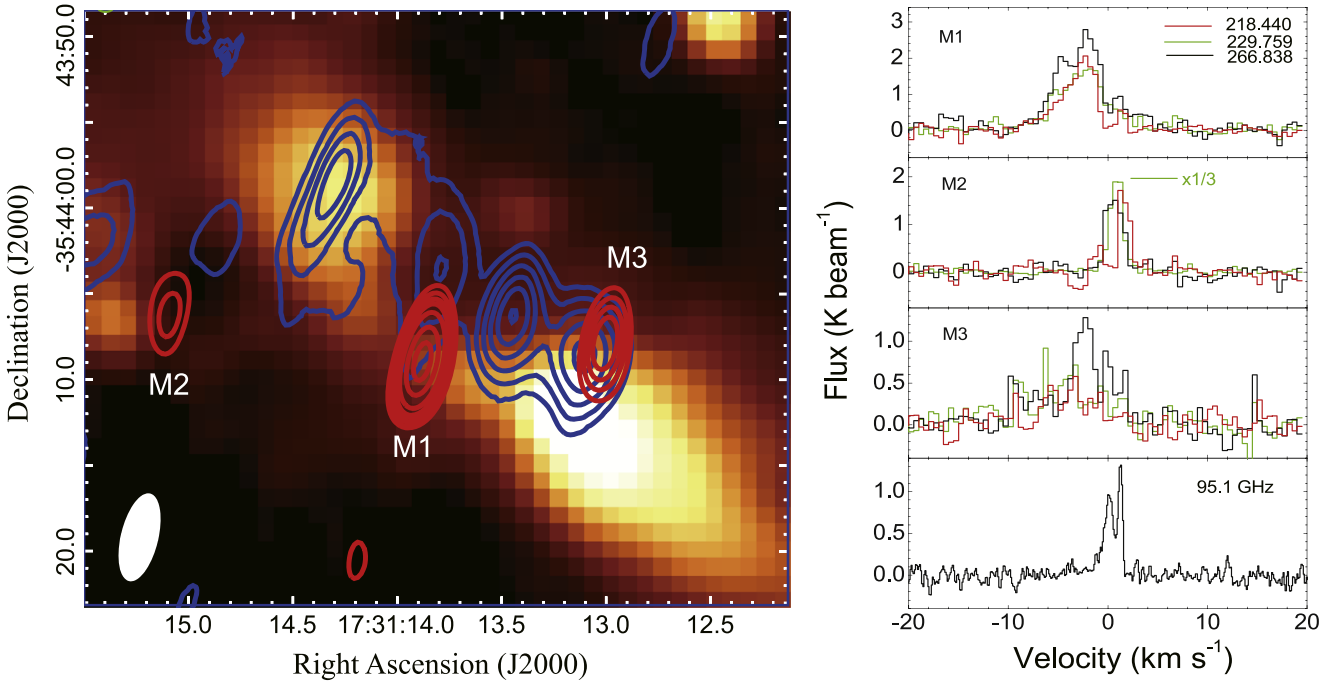

Figure 2. Comparison of the three class I methanol maser transitions with infrared and molecular shock tracers. The left panel shows the integrated emission from the 5_2-4_1E 266.8 GHz transition (red contours) overlaid on the near-infrared 2MASS K_s 2 μm image (background) and the integrated emission from the thermal $v = 0$ $J = 5-4$ 217.105 GHz SiO (blue contours). The contour levels are (3, 4, 5, 6, 8, 12, 16) $\times$ 0.5 Jy km s^{-1} beam^{-1} for the 266.8 GHz methanol emission and (3, 4, 5, 6, 7, 8, 9) $\times$ 0.5 Jy km s^{-1} beam^{-1} for the SiO emission. The right panel shows the methanol spectra from the 4_2-3_1 E 218.4 GHz (red), $8_{-1}-7_0$ E 229.7 GHz (green), and 5_2-4_1 E 266.8 GHz (black) transitions extracted toward the peak positions of the three methanol components M1 (α = 17:31:13.90, $\beta = -35$:44:08.9; J2000), M2 (α = 17:31:15.10, $\beta = -35$:44:06.0; J2000), and M3 (α = 17:31:13.00, $\beta = -35$:44:08.0; J2000) at the 266.8 GHz transition. Notably, the peak positions of the three transitions are same within the position errors of their images. The 95.1 GHz class I methanol maser spectrum from Chen et al. (2013a) is shown in the bottom of the right panel.

distributions at emission above $5\sigma_{\rm rms}$. The 2MASS near-infrared image shows extended emission in the 2 μm K_s-band, which is attributed to shock-excited H_2. Figure 2 shows that the 2 μm emission traces a bipolar-outflow structure elongated in the southwest to the northeast direction, with M1 located at the center and presumably associated with the driving source of the outflow. The integrated SiO emission also shows a bipolar structure, with a similar position angle to the 2 μm image. There is a close spatial correlation between the 2 μm and SiO emission in the northeastern section of the outflow, but less correspondence in the southwestern section. In the southwest, the SiO emission is located toward the edge of the bright 2 μm component. This may indicate that the SiO and 2 μm emission trace different shocked gas regions with different physical environments (such as different gas density and temperature), or may be due to variable extinction at near-infrared wavelengths.

The absence of tracers such as millimeter continuum emission or bright infrared point sources suggests that the M2 and M3 methanol emission regions are not directly associated with hot molecular cores (or protostars). In contrast, toward the M1 position significant millimeter continuum emission is detected in the current SMA observations (details of the continuum emission will be reported in a future paper). Figure 2 shows that the three class I methanol masers in the M3 region are closely associated with the shocked gas traced by the SiO and 2 μm emission, but offset toward the edge of the shocked gas region. Toward the M2 region there is no SiO emission detected and the methanol emission is also offset from a secondary 2 μm component (see Figure 2). The location of the M2 and M3 methanol regions toward the edge of the shocked gas is consistent with maser emission, because in such regions the shocks can produce stronger emission due to a larger coherence path along the line of sight.

Chen et al. (2013a) detected 95.1 GHz class I methanol maser emission toward G352.630-1.067 and the spectrum is shown at the bottom of the right panel in Figure 2. The 95.1 GHz methanol maser observations were made with the Mopra telescope (single-dish), which has a main-beam size of 36″ at this frequency (see Chen et al. 2013a). Figure 2 demonstrates the similarity of the emission from the M2 region in the 218.4, 229.8, and 266.8 GHz transitions with that observed from the 95.1 GHz methanol. In each case we observe a peak near $\sim$1 km s^{-1} and a narrow line width ($\sim$1.5 km s^{-1}). A secondary peak in the 95.1 GHz transition is seen at a velocity of $\sim$0 km s^{-1}, and we suggest that this may be mainly from the M3 region, because the 266.8 GHz emission from M3 shows a very similar profile in the velocity range 0–2 km s^{-1}. Notably, there is no significant emission from the 95.1 GHz transition at velocities less than -1 km s^{-1}, suggesting that there is no significant contribution from M1, which appears to be predominantly (or exclusively) thermal emission. At present we do not have any high-resolution observations of the 95.1 GHz methanol masers, so it is not possible to definitively determine if they are spatially coincident with M2 and M3. However, the spectra suggest that it is likely.

4. Discussion

4.1. Evidence for a Newly Identified Class I Maser Transition

Only the 4_2-3_1 E (218.4 GHz), $8_{-1}-7_0$ E (229.7 GHz), and 5_2-4_1 E (266.8 GHz) methanol transitions were detected

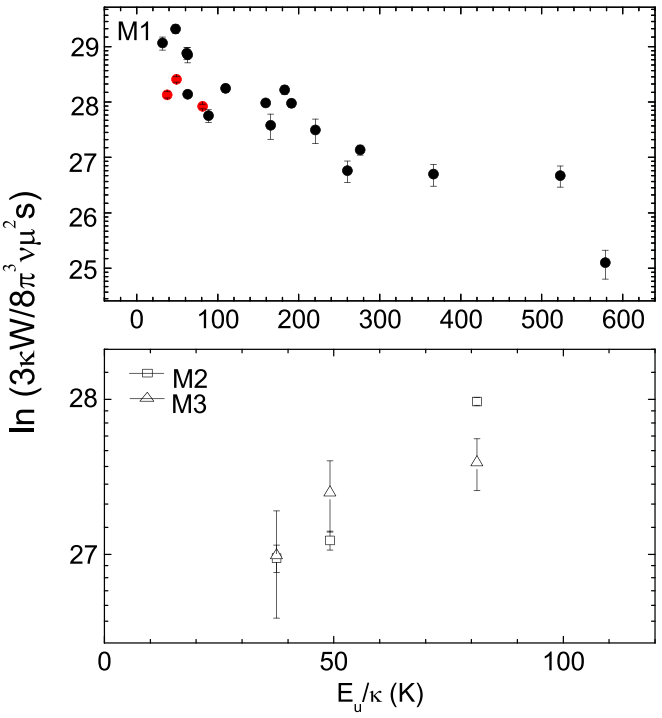

Figure 3. Rotation diagram for the methanol transitions from the current SMA observations. The upper panel shows the rotation diagram for M1, the three class I methanol maser transitions are represented with red circles, and other thermal transitions are marked with black circles. The lower panel shows the rotation diagram of the three class I transitions for M2 (squares) and M3 (triangles).

toward M2 and M3. The first two of these three transitions are known to be class I methanol maser transitions (Slysh et al. 2002; Hunter et al. 2014), and here in G352.630-1.067, we find that they are associated with shocked gas (see Figure 2). The 5_2-4_1 E (266.8 GHz) transition shows similar emission and spectral characteristics as the other two maser transitions, and the 266.8 and 218.4 GHz transitions belong to the same $J_2-(J-1)_1$ E series of transitions. Therefore, we suggest that the 5_2-4_1 E transition represents a newly identified class I maser transition. One point to note is that all of these methanol maser transitions have relatively low-energy upper levels (E_u = 37–81 K; see Table 1). This means that they can show thermal emission in a wide range of environments; however, in contrast to M1, there is no emission from other transitions with low upper-energy levels such as the $3_{-2}-4_{-1}E$, 230.0271 GHz (which has E_u = 32 K; Müller et al. 2005) toward either M2 or M3.

To investigate whether the emission from the 4_2-3_1 E (218.4 GHz), $8_{-1}-7_0$ E (229.7 GHz), and 5_2-4_1 E (266.8 GHz) methanol transitions is thermal, or due to a maser process we have performed rotation diagram analysis. The rotation diagram method is described in the Appendix. The rotation diagrams for the detected methanol transitions toward all three components are shown in Figure 3. It shows that all three class I transitions and the other thermal methanol transitions detected toward M1 show a trend in the rotation diagram consistent with thermal conditions. This also suggests that in M1 all the methanol transitions are predominantly produced by thermal emission. Actually, the best-fit straight line to the rotation diagram of the other thermal methanol lines detected toward M1 with the SMA observations gives an estimate of the rotational temperature of about 200 K (X. Chen et al. 2019, in preparation). This is consistent with M1 being a hot molecular core associated with the driving source for the outflows traced by the infrared 2 μm and thermal SiO emission (see Figure 2). In contrast, the three class I maser transitions show an inverse trend in the rotation diagram toward M2 and M3. This also suggests that the emission from these transitions toward M2 and M3 is not thermal, consistent with them all being class I methanol masers.

Figure 1 shows that the 4_2-3_1 E (218.4 GHz) and $8_{-1}-7_0$ E (229.7 GHz) transitions show stronger emission toward M2 than M3. In contrast, the newly identified maser transition (5_2-4_1 E 266.8 GHz) shows stronger emission at M3. Furthermore, the 5_2-4_1 E transition has a narrow spectral feature in addition to the broad spectral component seen in the other class I maser transitions (see Figure 2). These observations and the already mentioned secondary peak 10″ southeast of M1 seen in the 218.4 GHz line show that the maser emission from the three transitions had different characteristics, likely reflecting differing the physical environments for the M2 and M3 regions.

4.2. Model for the Three Class I Methanol Maser Transitions

In order to investigate the conditions under which a 266.8 GHz class I methanol maser can occur we have performed model calculations in the LVG (large velocity gradient) approximation. The details of the modeling procedure can be found in Sobolev & Deguchi (1994), Sobolev et al. (1997), and Cragg et al. (2002). The cosmic microwave background was assumed to be the only source for the external radiation field. For simplicity, we did not consider the dust emission and absorption within the maser region. A methanol level scheme including torsional quantum numbers up to $v_t = 2$ was used and the rates for collisions with para-H_2 and He were all the same as those used in Parfenov et al. (2016). The rates for collisions with ortho-H_2 were calculated in the same manner as in Nesterenok (2016).

The LVG model included the molecular hydrogen number density n_{H2}, methanol specific column density $N/\Delta V$, gas kinetic temperature T_{gas} and beaming factor $d(\ln r)/d(\ln V)$ as parameters. We investigated the brightness temperature of the three class I maser transitions over parameter ranges 10^4 cm^{-3} to $10^{8.5}$ cm^{-3}, 10^8–10^{14} cm^{-3} s and 50–300 K for n_{H2}, $N/\Delta V$ and T_{gas}, respectively, for two different values of $d(\ln r)/d(\ln V)$ (1 and 10). The results are summarized in Figure 4. The colored regions in Figure 4 show values of the physical parameters under which all three 218.4, 229.7, and 266.8 GHz maser transitions are inverted. The color in each plot shows the value of the maximal brightness temperature $T_{B,max}$, which for a fixed pair of parameters (e.g., n_{H2} and T_{gas} for the two lower plots in Figure 4), is the maximum of the brightness temperature achieved over the whole range of the third parameter ($N/\Delta V$ for the two lower plots).

Figure 4 shows that the three transitions are masing simultaneously for a wide range of physical parameters. The intensity of the masers greatly depends on the value of the beaming, as was noted by Sobolev & Parfenov (2018). The brightness temperature of the newly detected 266.8 GHz maser transition in our models only exceeds 10^3 K significantly for the higher value of the beaming factor (right plots in Figure 4).

In our analysis we did not search for the best-fit model because the available observational data do not provide enough constraints to be able to do this. Rather, we calculated the

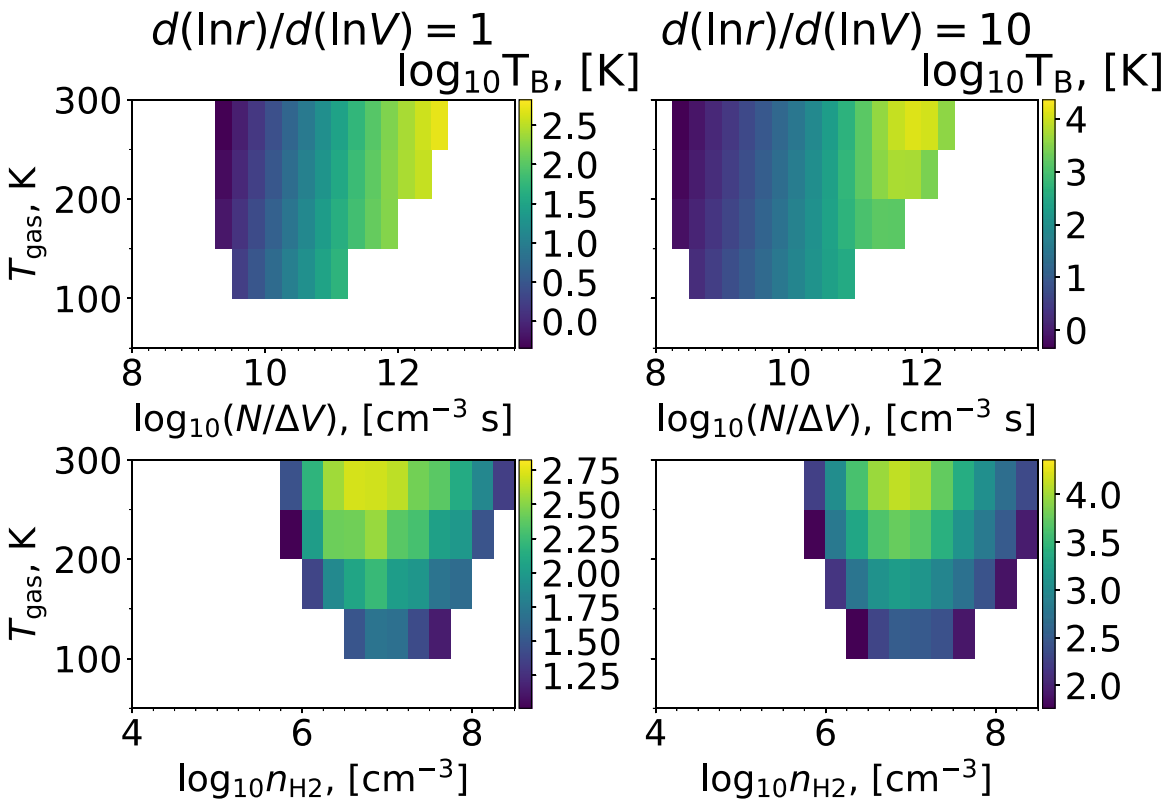

Figure 4. Maximum brightness temperatures of the 266 GHz transition according to LVG calculations described in the text. The lower panels show the maximum brightness temperature over the whole range of $N/\Delta V$ for the fixed values of n_{H2} and T_{gas}. The upper panels show the maximum brightness temperature over the whole range of n_{H2} for fixed values of $N/\Delta V$ and T_{gas}. The blank areas correspond to the case in which one of the three transitions at 218.4, 229.7, and 266.8 GHz is not masing. The left and right panels show the models calculated for the beaming factor values $d(\ln r)/d(\ln V) = 1$ and 10, respectively.

brightness temperatures for a fiducial model with $n_{H2} = 10^{7.0}$ cm^{-3}, $T_{gas} = 150$ K, $N/\Delta V = 10^{11.5}$ cm^{-3} s and beaming $d(\ln r)/d(\ln V) = 10$. These values are consistent with our current understanding of the physical conditions toward class I methanol maser sites (see, e.g., Voronkov et al. 2006 and Leurini et al. 2016). For these parameters the brightness temperatures of the 218.4 GHz, 229.7 GHz, and 266.8 GHz maser transitions are 2938 K, 6833 K, and 1234 K, respectively. These values significantly exceed the brightness temperature of all other methanol lines observed in the source. The intensity ratio for these brightness temperatures roughly corresponds to what is observed for these three transitions toward M2; however, it does not explain the ratios for M3 for which the 266.8 GHz line is the brightest. This may be a consequence of the simplicity of the current model, which does not take into account the structure of the maser source. However, the modeling undertaken demonstrates that the 218.4, 229.7 and 266.8 GHz class I methanol transitions can be the brightest methanol lines in the observed frequency range because they are masers for a broad parameter range.

We also checked the three H_2CO line transitions ($3_{03}-2_{02}$ 218.222 GHz, $3_{22}-2_{21}$ 218.475 GHz, and $3_{21}-2_{20}$ 218.760 GHz) surrounding the 4_2-3_1 E (218.4 GHz) methanol line, covered simultaneously in the observations. Assuming that the H_2CO emission is optically thin, the kinetic temperature of the gas in local thermodynamic equilibrium (LTE) can be derived with line-integrated intensity ratios $3_{22}-2_{21}/3_{03}-2_{02}$ or $3_{21}-2_{20}/3_{03}-2_{02}$ (e.g., Mangum & Wootten 1993; Tang et al. 2017a, 2017b, 2018a, 2018b). We measured the line-integrated intensity ratios $3_{22}-2_{21}/3_{03}-2_{02}$ or $3_{21}-2_{20}/3_{03}-2_{02}$ to be around 0.45 toward the three methanol regions M1, M2, and M3. Such ratios suggest that the kinetic temperature of the gas is around 200 K toward the maser regions, confirming our methanol simulations.

4.3. An Ideal Laboratory for Identifying New Methanol Masers: G352.630-1.067

The target source of the current observations, G352.630-1.067, has been measured to be at a distance of ~0.7 kpc from very long baseline interferometry parallax observations of the associated 6.7 GHz methanol maser (Chen et al. 2019). This makes it the second closest high-mass star formation currently known, with only the Orion Nebula (~400 pc; see Menten et al. 2007 and Kounkel et al. 2017) being closer. As one of the closest HMSFR, this potentially makes detections of masers easier than detections of more distant HMSFRs.

Chen et al. (2019) showed that G352.630-1.067 likely lies in an inter-arm region and furthermore it is in a relatively simple environment (either a small cluster or an isolated high-mass star). The infrared emission from 2MASS and GLIMPSE shows a clearly extended bipolar-outflow (angular scale 30″), which is also seen in the thermal SiO emission (see Figure 2). The emission from the three class I methanol masers toward the M2 and M3 regions is clearly associated with shocked gas. So G352.630-1.067 represents a good target for searching for new class I methanol masers transitions, particularly those in the same series that have been detected in E-type I methanol in the current observations. The 6.7 GHz class II methanol maser is clearly associated with the driving source of the extended outflow (Chen et al. 2019), the thermal hot core (M1).

Therefore M1, is potentially also a good target to search for new class II maser transitions at (sub-)millimeter wavelengths. High-angular-resolution observations with instruments such as ALMA are able to measure high brightness temperatures (>1000 K), effectively excluding the possibility of thermal emission associated with the hot molecular core (see for example Zinchenko et al. 2017).

5. Summary

SMA observations of the nearby HMSFR G352.630-1.067 have detected a new class I methanol maser from the 5_2-4_1 E transition (266.8 GHz). This new class I maser shows similar emission and spectral characteristics as the two previously known maser transitions, the 4_2-3_1 E (218.4 GHz) and $8_{-1}-7_0$ E (229.7 GHz) lines, which were also detected in the current observations. All three of these class I methanol masers are from the E-type methanol species. In contrast to other thermal methanol lines, which were only observed toward the hot core region, maser transitions were detected in two additional regions. These two maser regions are found to be associated with shocked gas traced by the 2 μm Ks-band and the thermal SiO molecular emission. A rotation diagram analysis shows a positive slope for the M2 and M3 regions where the three class I masers are detected. LVG modeling shows that the 266.8 GHz transition is masing for a wide range of physical parameters for which the 218.4 and 229.7 GHz transitions are also masers. The combination of these observational and modeling facts strongly suggests that the detected emission from the 5_2-4_1 E 266.8 GHz transition is masing toward the M2 and M3 regions. Due to its proximity and the simple environment, G352.630-1.067 provides an excellent target for identifying new methanol maser transitions.

We thank an anonymous referee for helpful comments that improved the manuscript. This work was supported by the National Natural Science Foundation of China (11590781, 11873002, 11590780) and Australian Research Council Discovery project number DP180101061 funded by the Australian Government. A.M.S. and S.P. were supported by the Russian Science Foundation (grant 18-12-00193).

Appendix
Rotation Diagram Analysis for the Multiple Methanol Transitions

Rotation diagrams assume that the molecular emission is optically thin and that the gas is in LTE. The standard formula for the rotation diagram analysis of optically thin lines can be derived from the following equation (e.g., Blake et al. 1987; Chen et al. 2013b):

$$\ln\left(\frac{3\kappa W}{8\pi^3\nu S\mu^2}\right) = \ln\frac{N}{Q} - \frac{E_u/\kappa}{T_{\rm rot}}. \quad (1)$$

where k is the Boltzmann constant in erg $\rm K^{-1}$, W is the observed line-integrated intensity of the species of interest in units of K km $\rm s^{-1}$, ν is the frequency of the transition in Hz, and $S\mu^2$ is the product of the total torsion-rotational line strength and the square of the electric dipole moment, E_u/k is the upper level energy in K, Q is the partition function at temperature $T_{\rm rot}$, and τ is the optical depth. The values of ν, $S\mu^2$, and E_u/k for each methanol transition can be found in Table 1. The partition function Q is given in the equation below for CH_3OH (e.g., Blake et al. 1987):

$$Q(T_{\rm rot}) = 1.2327T_{\rm rot}^{1.5}. \quad (2)$$

Under pure thermal conditions, a plot of $\ln(3\kappa W/8\pi^3\nu S\mu^2)$ versus E_u/κ will have a slope of $-1/T_{\rm rot}$ and an intercept of ln (N/Q).

ORCID iDs

Simon P. Ellingsen https://orcid.org/0000-0002-1363-5457

References

Blake, G. A., Sutton, E. C., Masson, C. R., & Phillips, T. G. 1987, ApJ, 315, 621
Breen, S. L., Ellingsen, S. P., Caswell, J. L., & Lewis, B. E. 2010, MNRAS, 401, 2219
Caswell, J. L., Fuller, G. A., Green, J. A., et al. 2010, MNRAS, 404, 1029
Chen, X., Ellingsen, S. P., Gan, C. G., et al. 2014, ChSBu, 59, 1066
Chen, X., Ellingsen, S. P., Shen, Z. Q., et al. 2011, ApJS, 196, 9
Chen, X., Gan, C.-G., Ellingsen, S. P., et al. 2013a, ApJS, 206, 9
Chen, X., Gan, C.-G., Ellingsen, S. P., et al. 2013b, ApJS, 206, 22
Chen, X., Li, J.-J., Zhang, B., et al. 2019, ApJ, 871, 198
Chipman, A., Ellingsen, S. P., Sobolev, A. M., & Cragg, D. M. 2016, PASA, 33, 56
Cragg, D. M., Johns, K. P., Godfrey, P. D., & Brown, R. D. 1992, MNRAS, 259, 203
Cragg, D. M., Sobolev, A. M., & Godfrey, P. D. 2002, MNRAS, 331, 521
Cragg, D. M., Sobolev, A. M., & Godfrey, P. D. 2005, MNRAS, 360, 533
Cyganowski, C. J., Brogan, C. L., Hunter, T. R., & Churchwell, E. 2009, ApJ, 702, 1615
Ellingsen, S. P. 2006, ApJ, 638, 241
Ellingsen, S. P., Sobolev, A. M., Cragg, D. M., & Godfrey, P. D. 2012, ApJL, 759, L5
Ellingsen, S. P., Voronkov, M. A., Breen, S. L., Caswell, J. L., & Sobolev, A. M. 2018, MNRAS, 480, 4851
Gan, C. G., Chen, X., Shen, Z.-Q., Xu, Y., & Ju, B.-G. 2013, ApJ, 763, 2
Green, J. A., Breen, S. L., Fuller, G. A., et al. 2017, MNRAS, 469, 1383
Green, J. A., Caswell, J. L., Fuller, G. A., et al. 2009, MNRAS, 392, 783
Hunter, T. R., Brogan, C. L., Cyganowski, C. J., & Young, K. H. 2014, ApJ, 788, 187
Kalenskii, S. V., Johansson, L. E. B., Bergman, P., et al. 2010, MNRAS, 405, 613
Kalenskii, S. V., Promyslov, V. G., Slysh, V. I., Bergman, P., & Winnberg, A. 2006, ARep, 50, 289
Kounkel, M., Hartmann, L., Loinard, L., et al. 2017, ApJ, 834, 142
Kurtz, S., Hofner, P., & Álvarez, C. V. 2004, ApJS, 155, 149
Leurini, S., Menten, K. M., & Walmsley, C. M. 2016, A&A, 592, A31
Mangum, J. G., & Wootten, A. 1993, ApJS, 89, 123
McCarthy, T. P., Ellingsen, S. P., Voronkov, M. A., & Cimó, G. 2018, MNRAS, 477, 507
Menten, K. M. 1991, ApJL, 380, L75
Menten, K. M., Reid, M. J., Forbrich, J., & Brunthaler, A. 2007, A&A, 474, 515
Müller, H. S. P., Schloder, F., Stutzki, J., & Winnewisser, G. 2005, JMoSt, 742, 215
Nakashima, J. I., Sobolev, A. M., Salii, S. V., et al. 2015, PASJ, 67, 95
Nesterenok, A. V. 2016, MNRAS, 455, 3978
Parfenov, S. Y., Semenov, D. A., Sobolev, A. M., & Gray, M. D. 2016, MNRAS, 460, 2648
Pihlström, Y. M., Sjouwerman, L. O., Frail, D. A., et al. 2014, AJ, 147, 73
Salii, S. V., Sobolev, A. M., & Kalinina, N. D. 2002, ARep, 46, 955
Sjouwerman, L. O., Pihlström, Y. M., & Fish, V. L. 2010, ApJL, 710, L111
Slysh, V. I., Kalenskiĭ, S. V., & Val'tts, I. E. 2002, ARep, 46, 49
Sobolev, A. M., Cragg, D. M., Ellingsen, S. P., et al. 2007, IAUS, 242, 81
Sobolev, A. M., Cragg, D. M., & Godfrey, P. D. 1997, A&A, 324, 211
Sobolev, A. M., & Deguchi, S. 1994, A&A, 291, 569
Sobolev, A. M., Ostrovskii, A. B., Kirsanova, M. S., et al. 2005, IAUS, 227, 174
Sobolev, A. M., & Parfenov, S. Y. 2018, IAUS, 336, 57
Sobolev, A. M., & Strelnitskii, V. S. 1983, SvAL, 9, 12
Tang, X. D., Henkel, C., Chen, C.-H. R., et al. 2017a, A&A, 600, 16

Tang, X. D., Henkel, C., Menten, K. M., et al. 2017b, A&A, 598, 30
Tang, X. D., Henkel, C., Menten, K. M., et al. 2018a, A&A, 609, 16
Tang, X. D., Henkel, C., Wyrowski, F., et al. 2018b, A&A, 611, 6
Voronkov, M. A., Brooks, K. J., Sobolev, A. M., et al. 2006, MNRAS, 373, 411
Voronkov, M. A., Caswell, J. L., Britton, T. R., et al. 2010a, MNRAS, 408, 133
Voronkov, M. A., Caswell, J. L., Ellingsen, S. P., et al. 2012, IAUS, 287, 433
Voronkov, M. A., Caswell, J. L., Ellingsen, S. P., Green, J. A., & Breen, S. L. 2014, MNRAS, 439, 2584
Voronkov, M. A., Caswell, J. L., Ellingsen, S. P., & Sobolev, A. M. 2010b, MNRAS, 405, 2471
Voronkov, M. A., Walsh, A. J., Caswell, J. L., et al. 2011, MNRAS, 413, 2339
Yanagida, T., Sakai, T., Hirota, T., et al. 2014, ApJL, 794, L10
Yang, W.-J., Xu, Y., Chen, X., et al. 2017, ApJS, 231, 20
Zinchenko, I., Liu, S.-Y., Su, Y.-N., & Sobolev, A. M. 2017, A&A, 606, L6